

Journal of Materials Chemistry A

Accepted Manuscript



This is an *Accepted Manuscript*, which has been through the Royal Society of Chemistry peer review process and has been accepted for publication.

Accepted Manuscripts are published online shortly after acceptance, before technical editing, formatting and proof reading. Using this free service, authors can make their results available to the community, in citable form, before we publish the edited article. We will replace this *Accepted Manuscript* with the edited and formatted *Advance Article* as soon as it is available.

You can find more information about *Accepted Manuscripts* in the [Information for Authors](#).

Please note that technical editing may introduce minor changes to the text and/or graphics, which may alter content. The journal's standard [Terms & Conditions](#) and the [Ethical guidelines](#) still apply. In no event shall the Royal Society of Chemistry be held responsible for any errors or omissions in this *Accepted Manuscript* or any consequences arising from the use of any information it contains.

Cite this: DOI: 10.1039/c0xx00000x

www.rsc.org/xxxxxx

ARTICLE TYPE

Hybrid acrylic/CeO₂ nanocomposites using hydrophilic spherical and high aspect ratio CeO₂ nanoparticlesMiren Aguirre,^a Eric Johansson Salazar-Sandoval,^{b,c} Mats Johansson^c, Anwar Ahniyaz,^b Maria Paulis^a and Jose Ramon Leiza^a⁵ Received (in XXX, XXX) Xth XXXXXXXXX 20XX, Accepted Xth XXXXXXXXX 20XX

DOI: 10.1039/b000000x

A dispersion of CeO₂ nanoparticles and nanorods stabilized with nitrilotriacetic acid (NTA) and 4,4'-Azobis(4-cyanovaleric acid) (V-501) initiator has been used to initiate the emulsion polymerization of acrylic monomers, yielding stable hybrid CeO₂ nanoparticles-nanorods/polyacrylate latexes for the first time. Films casted from these hybrid latexes are transparent due to the very homogenous
¹⁰ distribution of the polymer compatibilized CeO₂. Furthermore, it has been proven that the UV-Vis absorption capacity of the hybrid latexes is enhanced with the incorporation of the nanorods.

Introduction

It is well-known that inorganic nanomaterials have unique
¹⁵ properties that when combined appropriately with polymers, produce hybrid materials with substantially better performance (mechanical, optical, electrical...) ¹⁻⁴. In this context, cerium oxide possesses interesting properties such as the high UV-Vis absorbance capacity⁵. Thus, hybrid latexes with cerium oxide
²⁰ nanoparticles are potential candidates for the outdoor coating industry and for hybrid organic/inorganic photoactive layers in solar cells. Several works have already reported the synthesis of CeO₂/polymer hybrids for UV protection purposes⁶⁻⁸. However, all of them were produced with 3D CeO₂ nanoparticles; namely,
²⁵ spherical nanoparticles. The use of CeO₂ in photovoltaic applications has been scarce due to their wide band gap (≈3.19 eV), but recently doping or nanostructuring of this rare earth oxide has led to open the path to photoelectrochemical applications⁹.

³⁰ High aspect ratio materials attract more attention due to the fact that smaller amounts of these materials are enough to obtain similar characteristics¹⁰. Those materials exhibit great optical, mechanical, catalytic, and electrical properties that can be applied in a wide range of applications¹¹⁻¹³. In the last years, 1-D ceria nanostructures with different morphologies, for example
³⁵ nanorods, nanowires and/or nanotubes have been synthesized using a wide range of methods¹⁴⁻¹⁸.

Recently, it has been reported that with the combination of geometrically different nanofillers in a polymeric matrix,
⁴⁰ synergetic effects could be achieved. For instance, carbon nanotubes (CNTs) with carbon black¹², few-layered graphene with CNTs and nanodiamonds¹⁹, graphene and CNTs²⁰, PbS_xSe_{1-x} quantum dots and nanorods²¹ and also two different high aspect ratio materials; clay and CNTs²². In all of them a remarkable
⁴⁵ enhancement in the properties of the hybrids was observed.

Although many synthesis and surface modification methods for water dispersible ceria nanoparticles have been studied²³⁻²⁵, there have been many challenges in the successful incorporation of ceria nanoparticles into the polymer structure^{26,27}; for example, in

⁵⁰ clear coatings one of the key challenges is the stability of the paints formulated with ceria nanoparticles or in hybrid solar cells the power conversion efficiency is limited by the large-scale aggregation of the nanoparticles phase²⁸. Therefore, the inherent instability of inorganic particles in the organic matrix, makes it
⁵⁵ rather difficult to obtain stable dispersions from the physical mixture of inorganic nanoparticles and organic binders which often result in hazy films due to aggregation of nanoparticles²⁹. As a result, the in-situ incorporation of the ceria nanoparticles and other inorganic nanoparticles within the polymer particles
⁶⁰ during the polymerization process have been pursued in the last decade in order to homogeneously distribute the inorganic nanoparticles in the polymeric film³⁰⁻³⁶.

Several approaches to produce waterborne hybrid CeO₂/polymer coatings have been reported. We have recently shown the
⁶⁵ efficiency of a conventional seeded semibatch emulsion polymerization for the encapsulation of CeO₂ nanoparticles in waterborne polymer particles⁷. Hydrophobic CeO₂ nanoparticles were used and miniemulsion polymerization was employed to produce the seed hybrid particles. The monomer added under
⁷⁰ starved conditions buried the CeO₂ nanoparticles incorporated to the seed particles, producing a high homogeneity of nanoparticles dispersion in the final polymeric film. Other authors used macro-RAFT modified CeO₂ nanoparticle dispersions to start the
⁷⁵ polymerization^{35,37,36}. These modified particles were used as seed in an emulsion polymerization reaction that yielded an homogeneous distribution of the nanofiller in the final latex. The advantage of the hybrid latexes with encapsulated morphology with respect to hybrids produced by physically blending the bare
⁸⁰ dispersions of the inorganic and organic materials is that the possible aggregation of ceria nanoparticles during the storage period of the paint or film formation is prevented.

In this work, a dispersion of semiconductor cerium oxide nanoparticles (NP)/nanorods (NR) has been synthesized. During the synthesis of the CeO₂ nanoparticle dispersion in aqueous
⁸⁵ media, capping agents are usually added to stop the growth and hence, control the size of the nanoparticles. Generally, these capping agents (e.g. nitriloacetic acid, NTA; see structure in Figure)³⁸ contain carboxylic groups that are adsorbed onto the

surface of the growing inorganic nanoparticles stopping their growth and providing stability to the nanoparticle dispersion. In this work, and in order to enhance the compatibility and dispersability of the inorganic material in the polymer matrix, the possibility of modifying the surface of the CeO₂ nanoparticles by adding carboxylic acids containing initiator moieties that can initiate the polymerization from the surface of the CeO₂ nanoparticles was considered. Particularly, the acidic initiator 4,4'-Azobis(4-cyanovaleric acid) (V501) was used (see Figure 1) together with the NTA capping agent.

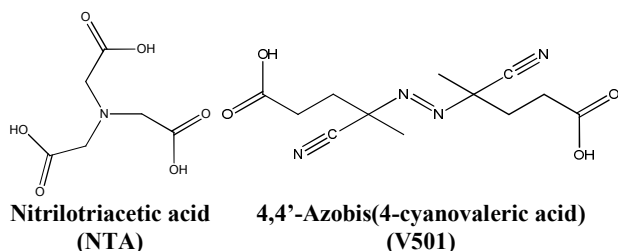


Figure 1. Chemical structures of NTA and V501 molecules.

Then, the polymerization from the surface of the CeO₂ nanoparticles was carried out in water phase in order to compatibilize the organic and the inorganic phases. Therefore the dispersion of the CeO₂ NP/NR was used as seed and initiator to produce hybrid acrylic latexes by emulsion polymerization. This is the first time that acrylic/CeO₂ nanorod/nanoparticle hybrids are reported in the literature. The stability of the final hybrid latexes, together with their final morphology was analyzed. Furthermore, the morphology and UV absorption capacity of hybrid polymeric films containing CeO₂ NP/NR was compared to those containing CeO₂ nanoparticles alone.

Experimental part

Materials

Cerium (III) nitrate hexahydrate (Ce(NO₃)₃·6H₂O), ammonium hydroxide solution (28.0-30.0%), nitrilotriacetic acid (NTA, 98+% ACS reagent), sodium nitrilotriacetate (Na₃NTA, Sigma grade) and 4,4'-Azobis(4-cyanovaleric acid) (V501) were purchased from Sigma-Aldrich and together with hydrogen peroxide (30%, MERCK) were used for the synthesis of the cerium oxide dispersion. Methyl methacrylate, MMA (Quimidroga) and n-Butyl acrylate, BA (Quimidroga) were used as monomers. Dodecyl diphenyloxide disulfonate (Dowfax 2A1 45%, Dow Chemicals) was used as the anionic emulsifier. Double distilled water was used for the synthesis of cerium oxide dispersion whereas deionized water was used in the emulsion polymerizations.

Synthesis of CeO₂ nanoparticles dispersions

The synthesis of hydrophilic nanoparticles/nanorods (NP/NR) dispersion was carried out as follows:

30 g of Ce (NO₃)₃·6H₂O were added to 300 mL of H₂O and stirred until complete dissolution. Then, 24 g of NH₄OH solution (28 wt%) were added to precipitate Ce(OH)_x. After centrifuging this mixture and eliminating the supernatant, the cerium hydroxide cake was redispersed in 1.5 L of H₂O previously heated at 85 °C using magnetic stirring and Ultra-Turrax® at high revolutions (ca. 10 000 rpm). The temperature was set to 88 °C while magnetic and Ultra-Turrax® stirrings were kept. When the cake chunks were not seen any longer, 4 g of NTA and 2 g of Na₃NTA were added to the reaction batch and it was left under

stirring for 15 minutes. After obtaining a homogeneous system, 8 g of H₂O₂ solution (30 wt%) were added to oxidize the cerium hydroxide (Ce(OH)_x) to cerium dioxide (CeO₂). 45 minutes after the addition of the peroxide, 3 g of Na₃NTA were added to the dispersion. This way the growth of CeO₂ particles was stopped by the NTA capping agent. During the following 15 minutes, stirring and temperature were maintained. Then, both heating and Ultra-Turrax® were turned off, while magnetic stirring was kept to help cooling down the system.

When the temperature of the dispersion was below 30 °C (to avoid the decomposition of the thermal initiator), 1.2 g of V501 (acidic azo initiator) were added, followed by the addition of one more gram of Na₃NTA. By the addition of V501, the exchange of some surface NTA units by V501 units was pursued. The final CeO₂ content of the dispersion was 1.6 wt%. The sample was stored at 3-4 °C to prevent the decomposition of the thermal initiator V501. The synthesized dispersion of nanoparticles was stable for more than one month in the refrigerator.

Polymerization of the acrylic/CeO₂ hybrid latexes

The polymerizations were carried out in a 100 mL glass jacketed reactor fitted with a reflux condenser, sampling device, N₂ inlet and a stirrer rotating at 200 rpm. In a typical experiment (see Run 1 in Table 1) the CeO₂ NP/NR aqueous dispersion (24.75 g) and water (74.25 g) were placed in the reactor. The feeding of the monomer (using a syringe pump, Fisher Scientific, 78-11001 Series) and the temperature heating were started simultaneously. The temperature was set to 75 °C. The monomer was fed for 150 minutes with a flow rate of 0.004 g/min for Run1. After 30 minutes the emulsifier was added in a shot dissolved in 2 mL of water. The total reaction time was of 210 minutes, namely after the monomer feeding, the polymerization was left to react for one more hour. No extra initiator was added to the polymerization reaction, apart from the one present in the CeO₂ NP/NR dispersion.

Table 1. Formulations used in the emulsion polymerization of the acrylic/CeO₂ NP/NR hybrid latexes.

	Initial reactor content		Monomer feed (150 min)		Shot (after 30 min)
	CeO ₂ NP/NR Dispersion (g)	Water (g)	MMA (g)	BA (g)	Dowfax (mg L ⁻¹) ^a
Run 1	24.75	74.25	1	-	67.5
Run 2	24.75	74.25	1	-	135
Run 3	24.75	74.25	1	1	135
Run 4	24.75	74.25	5	5	135

^a With respect to the total amount of water

In order to favor the initiation of the polymerization from the surface of the NP/NR in some experiments (not shown in Table 1) emulsifier was not used or was used well below the critical micellar concentration (CMC). Unfortunately, these experiments yielded large amounts of coagulum and hence higher emulsifier concentration was used to get stable latexes.

Characterization techniques

The morphology of the nanoparticles/nanorods (NP/NR) dispersion as well as the hybrid latex dispersion were analyzed by Transmission electron microscopy (TEM), TECNAI G2 20 TWIN (FEI), operating at an accelerating voltage of 200 KeV in a bright-field image mode. The samples were diluted to 0.5-1 wt% and dried in the fridge at 4 °C. Nanoceria particle and nanorods size distributions were obtained using Image Pro Plus 7.0 software on 500 particles of each kind.

For the surface characterization of the CeO₂ dispersion different analyses were carried out, lyophilizing, centrifuging and dialyzing the sample. Spectra/Por (MwCO: 12000-14000) was used as membrane for the dialysis. The entire dialysate volume was changed for fresh water at least once a day. Dialysis was allowed to run until the conductivity of the dialysate was close to that of the DDI water (2 µS/cm). The “clean” dispersion was kept in the fridge at 4 °C to avoid the decomposition of the thermal initiator V501.

The supernatant water of the centrifuged samples was characterized by ¹³C-NMR spectroscopy. Samples were dissolved in deuterated water (D₂O) and analyzed in a Bruker AVANCE-400 spectrometer 400 MHz for 9 hours.

XPS composition data and spectra were acquired on SPECS (Berlin, Germany) instrument equipped with Phoibos 150 1D-DLD analyzer and a monochromatic Al Kα X-ray source. Compositional survey and detail scans were acquired using pass energy of 80 eV. High resolution spectra were acquired using pass energy of 30 eV. The above data were taken at 90° takeoff angle. Data analysis was performed with Casa XPS 2.3.16 Software to fit the signals to Gauss-Lorentzian curves, after removing the background (Shirley). Energy correction was performed by using the C1s peak at 284.6 eV as reference. ATR-IR spectroscopy of the CeO₂ dispersion was carried out in a FTIR-ATR Perkin-Elmer RX1 Spectrometer.

The UV-Vis absorption measurements were carried out using a Shimadzu spectrophotometer (model UV-2550 230V). The measurements in the 250-600 nm range were done at room temperature on 50 µm films casted in Teflon panels at 23 °C and 55% of humidity. The thermal properties of the hybrids were analysed by Differential Scanning Calorimetry (DSC, Q2000, TA Instruments) and Thermogravimetric Analysis (TGA, Q500 V6.5 build 196 TGA instrument) measurements.

Results and discussion

Morphology and surface characterization of the CeO₂ NP/NR dispersion

In Figure 2 TEM micrographs of the aqueous CeO₂ nanoparticles dispersion are presented. It can be observed that both, spherical CeO₂ nanoparticles and nanorods were formed during the synthesis, and they were homogeneously dispersed in the aqueous phase.

The dimensions of 500 nanorods and nanoparticles were independently measured from the TEM images to compute the particle size distributions (PSDs) of each population (Figure 2 and Supporting Information for the detailed PSDs). Nanorods dimensions were in the range 25-275 nm in length and 1-15 nm in width, with an average aspect ratio of 16. Nanoparticles sizes between 1-15 nm were measured with a volume average diameter of 6 nm.

Figure 3 describes the different steps carried out to characterize the surface of the NP and NR. In a first step, the CeO₂ dispersion was lyophilized and analyzed by XPS. It should be mentioned, that this sample was used as a reference because it should contain all the V501 initiator. The powder was redispersed in water and it was seen that it initiated the polymerization of MMA (see details in next sections).

On the other hand, in order to check if the initiator was adsorbed on the surface of the NP and NR, a fraction of the NP/NR dispersion was centrifuged at 10 °C, 20000 rpm and for 30 minutes. A fraction of the precipitated sample was analyzed by XPS and the supernatant of the centrifugation was analyzed by ¹³C-NMR.

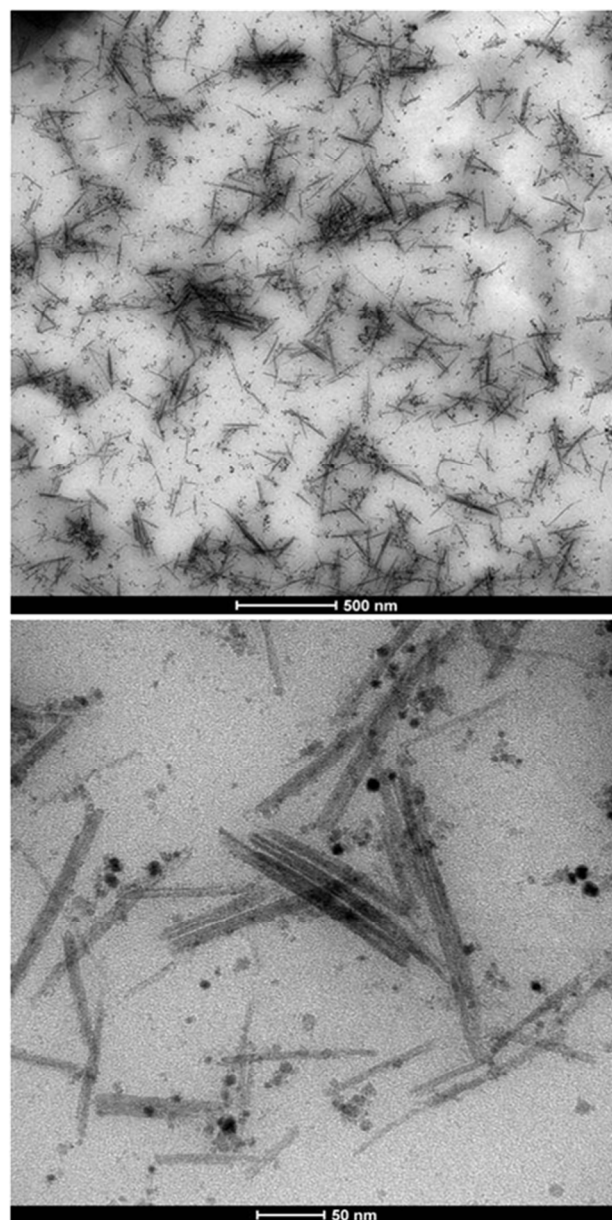


Figure 2. TEM micrographs of the CeO₂ nanoparticles dispersion containing spherical nanoparticles and nanorods.

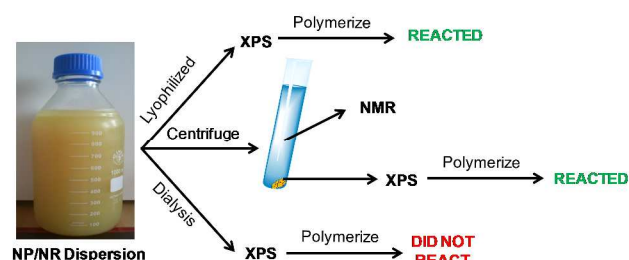


Figure 3. Experimental procedure followed to analyze the NP/NR dispersion.

Figure 4 presents the XPS analysis of the reference and the centrifuged sample, together with the pure V501. For the sake of clarity only the carbon and nitrogen component spectrum are displayed in Figure 4.

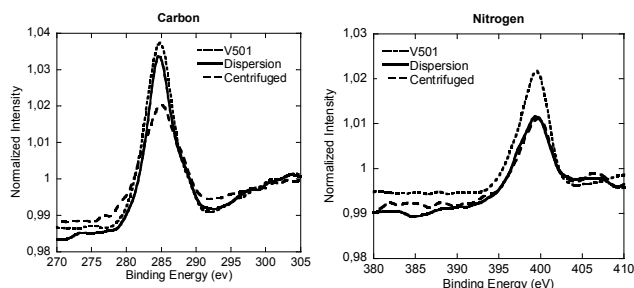


Figure 4. Normalized XPS spectra for the carbon and nitrogen components of the lyophilized CeO₂ dispersion, the centrifuged sample and V501.

As it can be seen in Figure 4, the peaks of V501, original dispersion and centrifuged samples, for C and N signals, are very similar. Although the peaks of the centrifuged sample were slightly shifted, the components detected in V501 were in good agreement with the peaks of the original dispersion and centrifuged samples (the binding energies of each component together with the deconvoluted spectra are shown in the Supporting Information), which means that the initiator was at least partially associated with the NP/NR surfaces.

The precipitated sample was redispersed in water and used to initiate the polymerization of MMA. The sample was still able to polymerize MMA (19% of conversion was achieved). This further supports our XPS results and confirms that a fraction of the initiator was present in the NP/NR surface after centrifugation.

The composition of the supernatant obtained after the centrifugation was analyzed by NMR. Figure 5 shows the ¹³C-NMR spectra and the chemical structures of the NTA and V501 species. The assignments of the peaks are described in detail in the Supporting Information. The spectrum confirms the presence of both, NTA and V501 in the aqueous phase after the centrifugation.

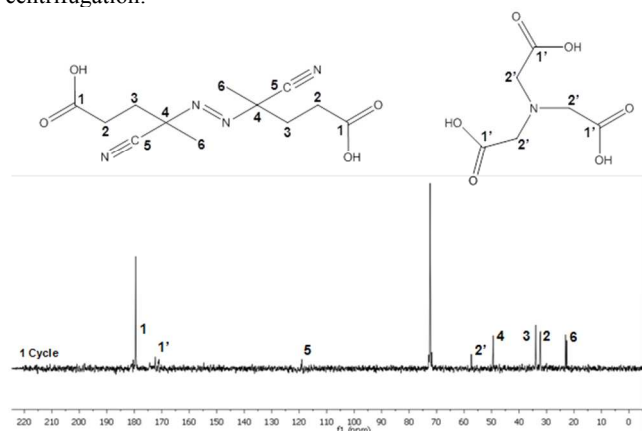


Figure 5. ¹³C-NMR spectra corresponding to the supernatant water of the centrifuged CeO₂ dispersion sample.

These results indicate that the V501 initiator might be partitioned between the surface of the NP/NR and the aqueous phase since it was detected in both phases; the centrifuged solid (XPS, MMA initiation) as well as in the supernatant (NMR).

In order to check this partition, the equilibrium of V501 was shifted to the aqueous phase by dialysis (Figure 3). The XPS spectrum of the dialyzed and initial sample is presented in Figure 6. It can be said that the V501 signals in the dialyzed sample were weaker and with more noise than those presented before. Moreover, it was confirmed that this sample was not able to

initiate the polymerization of MMA. It can be concluded that there was no initiator left on the surface of the CeO₂ NP/NR after the dialysis.

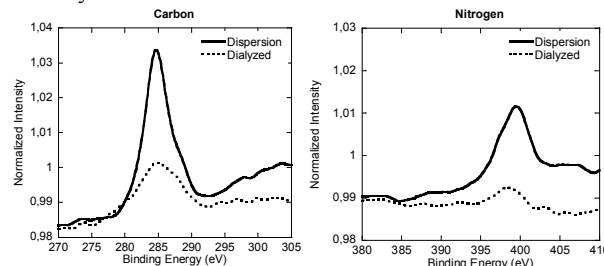


Figure 6. Normalized XPS spectra for the carbon and nitrogen components of the lyophilized CeO₂ dispersion and the dialyzed sample.

In order to better characterize the association of V501 with the CeO₂ surface, the Attenuated Total Reflectance Fourier transformed Infra Red spectroscopy (ATR-FTIR) was performed for the NP/NR dispersion and for pure NTA and V501. Figure 7 presents the results obtained. It can be seen that as already presented for the adsorption of NTA³⁸, the C=O band of the carboxylic groups from NTA and V501 (1720, 1708 cm⁻¹) are shifted to lower wavelengths (1565 cm⁻¹), demonstrating their chelation to the CeO₂ surface. Only a small fraction of carboxylic groups appear unshifted, which supports the amount of NTA and V501 found by NMR in the supernatant.

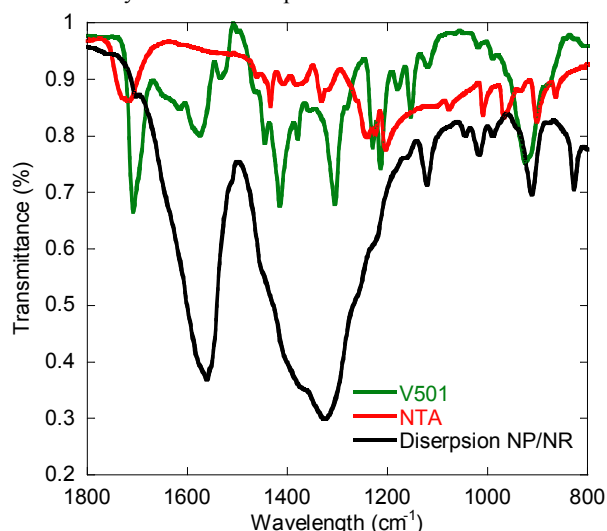


Figure 7. ATR-FTIR (Attenuated total reflectance-Fourier Transformed Infra Red spectroscopy) measurements for pure V501 and NTA, and for the NP/NR dispersion.

Therefore the characterization of the NP/NR indicates that V501 was associated in the surface of the NP/NR and that it is sufficient to start the polymerization of MMA without adding further initiator. The results also confirm that there exists an equilibrium between the acidic species (NTA and V501) at the surface of the nanoparticles and in the aqueous phase.

Emulsion polymerization in the presence of the V501 modified CeO₂ NP/NR dispersion

Semibatch emulsion polymerization reactions using the NP/NR dispersions and MMA or MMA/BA mixtures as monomers without further addition of initiator were carried out. The surfactant amount added in Run 1 was just below the cmc (critical micellar concentration, 70 mg/L³⁹) to minimize nucleation of particles and favor initiation from the surface of

CeO₂ NP/NRs. However, it was observed that under this condition unstable latexes were obtained. Only when the amount of surfactant was twice the cmc, stable latexes could be obtained (see runs 2-4 in Table 1).

Table 1. Stability, final solids content (referred to the polymer) and CeO₂ content for different hybrid acrylic/CeO₂ latexes obtained by emulsion polymerization.

	Final SC (%)	CeO ₂ (wbp %) ^a	dp (nm) ^b	Dowfax	Stability
Run 1	-	18.7		< cmc	Unstable
Run 2	1	18.7	31	> cmc	Stable
Run 3	2	9.4		> cmc	Stable
Run 4	5	3.7	83	> cmc	Stable

^a Weight based in polymer

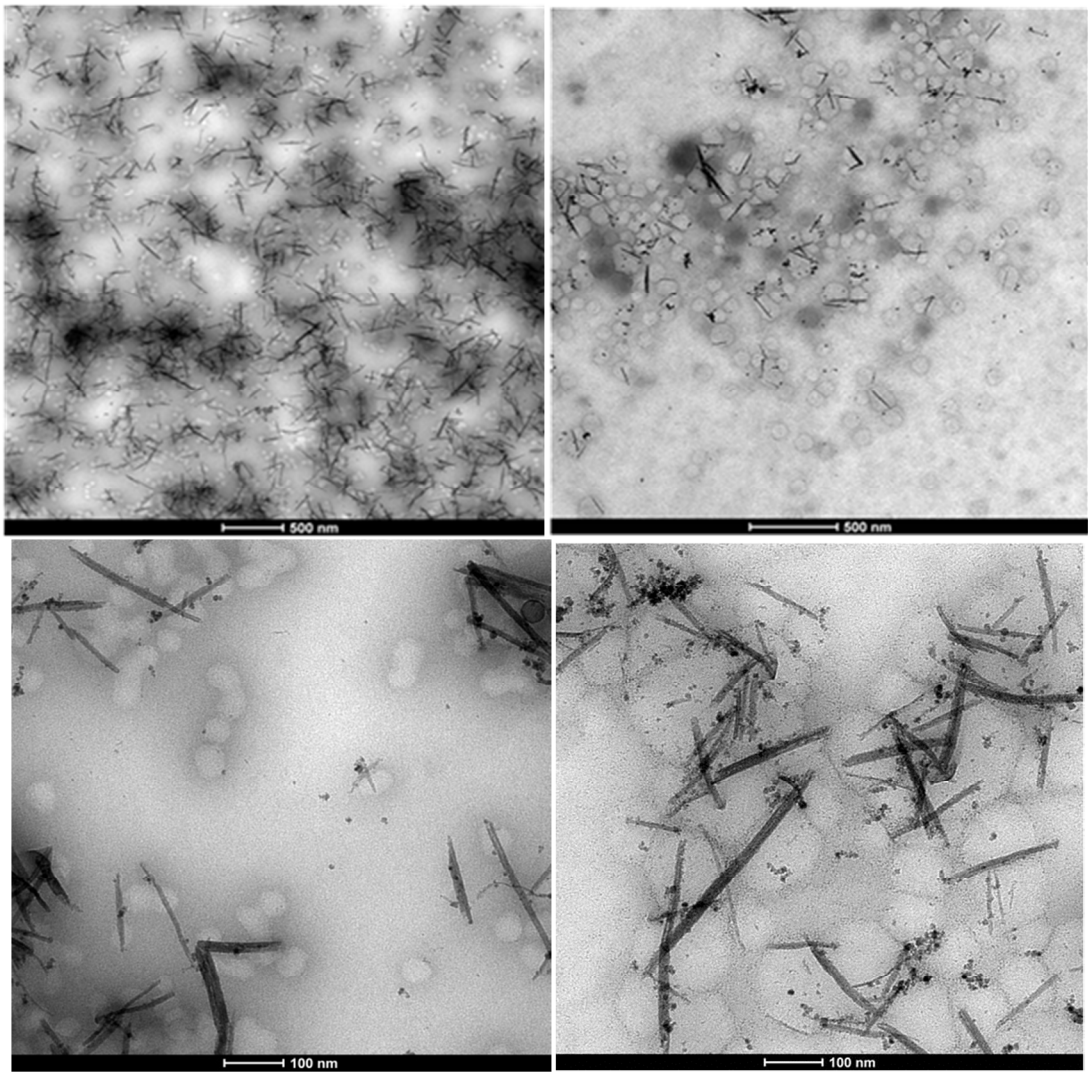
^b Volume average polymer particle size measured by TEM

In Run 2 (MMA) total conversion was achieved even if no extra initiator was added apart from the one present in the CeO₂ dispersion, whereas in Run 3 (MMA/BA) 90% conversion was reached. On the other hand, in Run 4, 50% conversion was

attained. The volume average polymer particle size measured by TEM was 31 nm for Run 2 and 83 nm for Run 4 (see Supporting Information). The size difference is related to the higher solids content of Run 4. Furthermore, the molecular weight distribution of Run 4 has also been measured, presenting a weight average molecular weight of 5.1x10⁵ g/mol with a polydispersity of 4.1, which are in the typical range of polymers produced by emulsion polymerization. Therefore, stable hybrid acrylic/CeO₂ NP/NR latexes with low solids content and CeO₂ contents between 3.7 and 18.7 wt% with respect to the polymer were successfully produced by this approach.

Morphology of the hybrid latexes containing CeO₂ NP/NR

Figure 8 presents the TEM micrographs of Run 2 and Run 4 hybrid latexes containing CeO₂ NP/NR. It can be clearly distinguished that the NP/NR concentration was higher in Run 2 (18.7% with respect to the polymer) than in Run 4 (3.7% with respect to the polymer).



Run 2 **Run 4**
Figure 8. TEM micrographs of the hybrid latexes for Run 2 and Run 4.

With regards to the location of the polymer particles, it seems that a large number of them are not associated to CeO₂ NP/NR, while there are others closer or attached to CeO₂ NP/NR. In the latter case the images are not conclusive to elucidate whether the polymerization initiated from the surface of the NP/NRs or the attachments of the polymer particles and NP/NRs occurred during the sample preparation for TEM.

Nonetheless, the TEM images are conclusive with regards to the occurrence of homogeneous or micellar nucleation, since a large number of free polymer particles (85%, counting 200 polymer particles), which apparently did not contain any CeO₂ moieties were identified. It seems that the concentration of emulsifier (above the CMC to ensure stability of the latex) and the partition of V501 initiator between the CeO₂ surface and the aqueous phase were significant enough to produce CeO₂-free polymer particles. Note that the only initiator present was the one used in the synthesis of the CeO₂ dispersion.

Films morphology and properties

In order to check the film forming properties of the hybrid latexes, films for Run 3 and Run 4 (MMA/BA, 50/50 wt%) were casted at room temperature for 24 hours (Figure 9). Good quality films (crack and voids free) were formed despite the low solids content. The films obtained were yellowish but transparent and the color increased with the CeO₂ content.

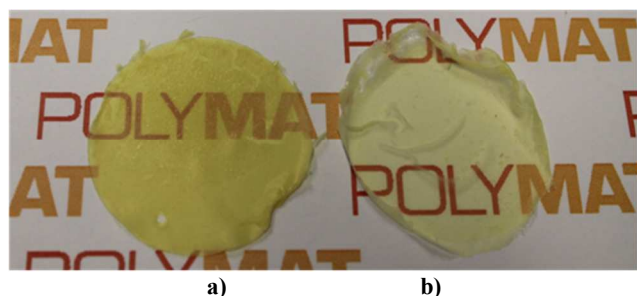


Figure 9. Films of a) Run 3 and b) Run 4 both casted at room temperature.

A TEM image of the hybrid film for Run 4 is presented in Figure 10. It can be seen that after film formation the NP/NR are still well dispersed and they did not tend to form aggregates. This is one of the main reasons to obtain transparent films. Therefore the main objective of the work was fulfilled as by the modification of the surface of the CeO₂ nanoparticles and nanorods, a good compatibility between the inorganic and the polymeric phase was achieved, obtaining a good dispersion of the inorganic material in the polymeric film. It must be pointed out that Runs 2-4 showed much higher stability than a physical blend of the CeO₂ dispersion and a blank latex (see Supporting Information), indicating that even if the amount of polymer grown from the surface of the CeO₂ nanoparticles was not large, it was enough to enhance the inorganic/organic compatibility.

Due to the high UV absorbance capacity of the CeO₂, the UV-Vis absorption of these films could not be measured directly because at the minimum achievable thickness of the films the transmission of UV-Vis light was completely blocked in the spectrophotometer. Alternatively, and in order to check if the CeO₂ particle shape has any effect on the UV absorption capacity, the hybrid latex synthesized in this work, Run 4, was blended (magnetically stirring for 1 h) with a blank latex to yield a hybrid latex with a final CeO₂ content of 1 wt% (Hybrid latex

NP/NR). The absorption of this film was compared to the blank film (0% CeO₂) and to a hybrid film containing only spherical CeO₂ nanoparticles (1 wt% CeO₂, Hybrid latex NP) prepared in a previous work⁷.

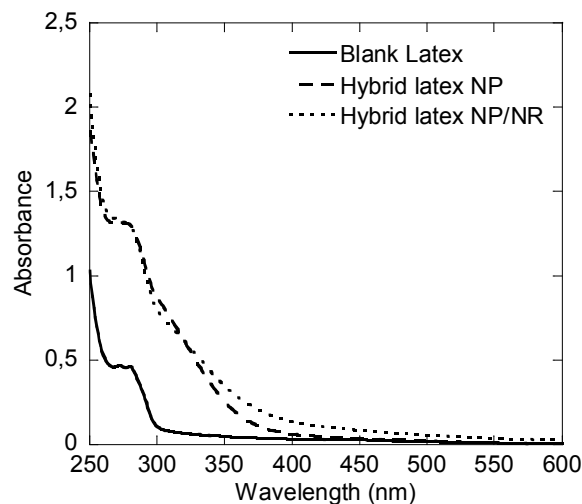
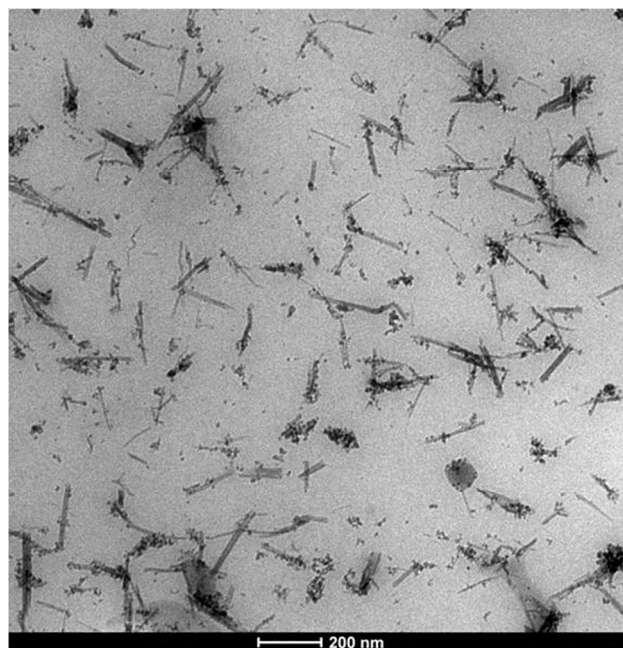


Figure 11. UV-Vis absorption capacity for the hybrid latexes prepared with 1 wt% of CeO₂ NP or NP/NR, compared to a blank latex.

Figure 11 presents the UV absorbance of the hybrids and the pristine latex films. It was observed, that the films containing CeO₂ performed considerably better than the pristine latex. However, in the dispersion that contained the nanorods, the UV absorption was enhanced at wavelengths above 350 nm, with respect to the dispersions that only contained spherical CeO₂ nanoparticles. In both of them the CeO₂ percentage was 1 wt% and therefore, the difference must come from the CeO₂ rod-like structures prepared in this work.

Furthermore the thermal properties of the films were also measured by DSC and TGA. Three different sample types have

been analyzed in order to check the effect of the amount and aspect ratio of the CeO₂ in the hybrids: a blank polymer (obtained from a blank latex without CeO₂), nanocomposites obtained by in-situ polymerization with 1 and 2 wt% of spherical⁴⁰ and the nanocomposite from Run 4, which contains 3.7% of NP/NR. It was observed that the glass transition temperature (T_g) of the three samples was within the range 14–16°C, which suggests a negligible effect of the amount and aspect ratio of the CeO₂ in the range studied (see the Supporting Information). The TGA showed that the thermal stability decreased slightly with the CeO₂ content. However, there were not big differences between the films containing NP or the one with NP/NR. The T₅₀ (temperatures for 50% of degradation) for the three samples were 350°C for the blank sample, 343°C for the hybrid containing 1 wt% of CeO₂ NP, 341°C for the hybrid containing 2 wt% of CeO₂ NP and 332°C for the hybrid containing 3.7 wt% of CeO₂ NP/NR (see the Supporting Information).

Conclusions

The emulsion polymerization of the dispersion of CeO₂ NP/NR with acrylate monomers, without further addition of initiator, led to stable hybrid latexes when the amount of emulsifier was above the cmc. Therefore, a hypothetical nucleation mechanism was proposed in which the polymerization could be started from both, the surface of the NP/NRs or from the aqueous phase. This is the first time that high aspect CeO₂ nanoparticles have been incorporated in polymer hybrids. Furthermore they produced good quality and transparent films at room temperature, due to the enhanced compatibility between the CeO₂ and the polymer, which prevented the CeO₂ aggregation during film formation. In addition, it has been proven that the UV-Vis absorption capacity was enhanced with the use of a mixture of different aspect ratio CeO₂, with no significant changes in the thermal properties. Furthermore this hybrid morphology with a opens also the way to new applications in the field of hybrid photoactive layers in solar cells, if the CeO₂ band gap is accordingly engineered.

Acknowledgements

Financial support from the European Union (Woodlife project FP7-NMP-2009-SMALL-246434) is gratefully acknowledged. Miren Aguirre thanks the Basque Government for the scholarship “Ikertzaileak prestatzeko eta hobetzeko laguntzak”. The sGIKer UPV/EHU is acknowledged for the electron microscopy facilities of TEM and X-ray measurements (XPS).

Notes and references

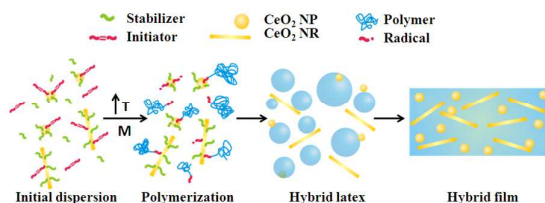
- ^a POLYMAT and Kimika Aplikatua saila, University of the Basque Country UPV/EHU, Joxe Mari Korta Zentroa, Tolosa Hiribidea 72, 20018 Donostia-San Sebastián, Spain.
jrleiza@ehu.es maria.paulis@ehu.es
- ^b SP Technical Research Institute of Sweden, Chemistry, Materials and Surfaces, Box 5607, SE-114 86, Stockholm, Sweden.
- ^c Department of Fibre and Polymer Technology, School of Chemical Science and Engineering, KTH Royal Institute of Technology, SE-100 44 Stockholm, Sweden.
- [†] Electronic Supplementary Information (ESI) available: It contains data on the particle size distribution of CeO₂ nanoparticles and nanorods, ¹³C-NMR and XPS data assignments, the particle size distribution of the polymer particles, the stability tests and the DSC and TGA measurements. See DOI: 10.1039/b000000x/

1. J. Hu, M. Chen, and L. Wu, *Polym. Chem.*, 2011, **2**, 760.
2. K. Landfester, *Angew. Chem. Int. Ed. Engl.*, 2009, **48**, 4488–4507.
3. M. Paulis and J. R. Leiza, ed. V. Vittal, Nova Science, 2010.
4. C. K. Weiss and K. Landfester, *Hybrid Latex Part.*, 2010, **233**, 185–236.
5. R. Li, S. Yabe, M. Yamashita, S. Momose, S. Yoshida, S. Yin, and T. Sato, *Solid State Ionics*, 2002, **151**, 235–241.
6. T. Masui, M. Yamamoto, T. Sakata, H. Mori, and G. Y. Adachi, *R. Soc. Chem.*, 2000, **10**, 353–357.
7. M. Aguirre, M. Paulis, and J. R. Leiza, *J. Mater. Chem. A*, 2013, **1**, 3155–3162.
8. M. Aguirre, M. Paulis, J. R. Leiza, T. Guraya, M. Iturrondobeitia, A. Okariz, and J. Ibarretxe, *Macromol. Chem. Phys.*, 2013, **214**, 2157–2164.
9. X. Lu, D. Zheng, P. Zhang, C. Liang, P. Liu, and Y. Tong, *Chem. Commun.*, 2010, **46**, 7721–7723.
10. P. C. Ma, M. Y. Liu, H. Zhang, S. Q. Wang, R. Wang, K. Wang, Y. K. Wong, B. Z. Tang, S. H. Hong, K. W. Paik, and J. K. Kim, *ACS Appl. Mater. Interfaces*, 2009, **1**, 1090–6.
11. E. Bourgeat-Lami and M. Lansalot, *Adv. Polym. Sci.*, 2010, **233**, 53–123.
12. E. D. Laird and C. Y. Li, *Macromolecules*, 2013, **46**, 2877–2891.
13. B. R. Saunders and M. L. Turner, *Adv. Colloid Interface Sci.*, 2008, **138**, 1–23.
14. G. Chen, C. Xu, X. Song, W. Zhao, Y. Ding, and S. Sun, *Inorg. Chem.*, 2008, **47**, 723–728.
15. K. S. Lin and S. Chowdhury, *Int. J. Mol. Sci.*, 2010, **11**, 3226–3251.
16. C. Sun, H. Li, H. Zhang, Z. Wang, and L. Chen, *Nanotechnology*, 2005, **16**, 1454–1463.
17. A. Vantomme, Z. Y. Yuan, G. Du, and B. L. Su, *Lagmuir*, 2005, **21**, 1132–1135.
18. B. Tang, L. Zhuo, J. Ge, G. Wang, Z. Shi, and J. Niu, *Chem. Commun.*, 2005, 3565–3567.
19. K. E. Prasad, B. Das, U. Maitra, U. Ramamurty, and C. N. R. Rao, *Prog. Nat. Acad. Sci.*, 2009, **106**, 13186.
20. C. Zhang, S. Huang, W. W. Tjiu, W. Fan, and T. Liu, *J. Mater. Chem.*, 2012, **22**, 2427–2434.

21. M. Nam, S. Kim, S. W. Kim, and K. Lee, *Nanoscale*, 2013, **5**, 8202–8209.
22. C. Tang, L. Xiang, J. Su, K. Wang, C. Yang, Q. Zhang, and Q. Fu, *J. Phys. Chem. B*, 2008, **112**, 3876–3881.
23. L. Qi, A. Sehgal, J. C. Castaing, J. P. Chapel, J. Fresnais, J. F. Berret, and F. Cousin, *ACS Nano*, 2008, **2**, 879–888.
24. J. Fresnais, C. Lavelle, and J. F. Berret, *J. Phys. Chem. C*, 2009, **113**, 16371–16379.
25. B. Chanteau, J. Fresnais, and J. F. Berret, *Langmuir*, 2009, **25**, 9064–70.
26. J. F. Berret, *Macromolecules*, 2007, **40**, 4260–4266.
27. L. Qi, J. P. Chapel, J. C. Castaing, J. Fresnais, and J. F. Berret, *Langmuir*, 2007, **23**, 11996–11998.
28. R. Rhodes, M. Horie, H. Chen, Z. Wang, M. L. Turner, and B. R. Saunders, *J. Colloid Interface Sci.*, 2010, **344**, 261–271.
29. S. Bardage, M. Henriksson, S. Olsson, P. Collins, D. Meng, A. Ahniyaz, E. Johansson, A. Rahier, M. Gasparini, and N. Lamproye, *Surf. Coat. Int.*, 2013, **2**.
30. B. Erdem, E. D. Sudol, V. L. Dimonie, and M. S. El-Aasser, *J. Polym. Sci. Part A Polym. Chem.*, 2000, **38**, 4441–4450.
31. H. Lu, B. Fei, J. H. Xin, R. Wang, and L. Li, *J. Colloid Interface Sci.*, 2006, **300**, 111–116.
32. N. Bechthold, F. Tiarks, M. Willert, K. Landfester, and M. Antonietti, *Macromol. Symp.*, 2000, **151**, 549–555.
33. J. Ramos and J. Forcada, *Langmuir*, 2011, **27**, 7222–7230.
34. Y. Mori and H. Kawaguchi, *Colloids Surf. B. Biointerfaces*, 2007, **56**, 246–254.
35. J. Garnier, J. Warnant, P. Lacroix-Desmazes, P. E. Dufils, J. Vinas, Y. Vanderveken, and A. M. Van Herk, *Macromol. Rapid Commun.*, 2012, **33**, 1388–92.
36. N. Zgheib, J. L. Putaux, A. Thill, E. Bourgeat-Lami, F. D’Agosto, and M. Lansalot, *Polym. Chem.*, 2013, **4**, 607.
37. N. Zgheib, J. L. Putaux, A. Thill, F. D’Agosto, M. Lansalot, and E. Bourgeat-Lami, *Langmuir*, 2012, **28**, 6163–74.
38. E. Johansson Salazar-Sandoval, M. K. G. Johansson, and A. Ahniyaz, *RSC Adv.*, 2014, **4**, 9048–9055.
39. I. de F. A. Mariz, *High Solids Content Low Viscosity Latexes with Small Particle Size*, 2011.
40. M. Aguirre, M. Paulis, and J. R. Leiza, *Polymer*, 2014, **55**, 752–761.

Hybrid acrylic/CeO₂ nanocomposites using hydrophilic spherical and high aspect ratio CeO₂ nanoparticles

Miren Aguirre,^a Eric Johansson Salazar-Sandoval,^{b,c} Mats Johansson^c, Anwar Ahniyaz,^b Maria Paulis^a and Jose Ramon Leiza^a



High aspect ratio CeO₂ nanoparticles have been incorporated in waterborne acrylic polymer hybrids for the first time.